Experimental Study on Cellular Premixed Propane Flames in a Narrow Gap between Parallel Plates

M. M. Alexeev[a], O. Yu. Semenov[a] and S. E. Yakush[b,c]

[a]Surgut State University, Ave. Lenina 1, Surgut 628400, Russia; [b]Ishlinskiy Institute for Problems in Mechanics RAS, Ave. Vernadskogo 101 Bldg 1, Moscow 119526, Russia; [c]Moscow Institute of Physics and Technology, 9 Institutsky Per., Dolgoprudniy 141701, Russia

ARTICLE HISTORY
Compiled January 22, 2019

ABSTRACT

Experimental results on laminar propane flames propagating in a narrow gap between parallel glass plates are presented. Development and evolution of cellular flame structure is demonstrated by video and long-exposure photo recordings for stoichiometric and fuel-rich mixtures with equivalence ratio of 1.0 to 1.25. It is shown that in narrow gaps the lateral cell sizes by far exceed the gap width. Average flame propagation speed obtained for gap widths between 2.5 and 4.4 mm is shown to depend significantly on the gap width due to the effect of heat losses on the normal flame speed, as well as due to cooling of products behind the flame. Effect of gap width on the cellular structure is demonstrated, and statistical characteristics of the cells are obtained for two gap widths. Flame propagation patterns are also obtained for non-central ignition performed at one or simultaneously at two points.

KEYWORDS

Laminar flame; channel flow; instability; cells; experiments; visualization

1. Introduction

Recent years have seen an increasing attention to the phenomena accompanying premixed combustion in narrow channels and gaps of different aspect ratios. To a large extent, this interest has been stimulated by the development of micro-combustors, micro-engines, thrusters, and other small-scale devices (Ju and Maruta 2011). Flame propagation in narrow gaps is featured by higher flow drag and stronger thermal interaction between the combustion zone and channel walls in comparison with conventional combustor due to much higher surface-to-volume ratio. In typical experimental configurations aimed at micro-combustor applications, gas was permanently supplied at the center of one plate, with combustion products outflowing at the periphery; the characteristic sizes of combustors were of the order of 0.05-0.1 m, with the gap width of few millimeters. Oscillating and rotating flames in radial micro-channels with one heated wall were studied extensively by Minaev *et al.* (2007); Fan *et al.* (2008, 2009); Minaev *et al.* (2013) where specific flame patterns were obtained experimentally and

Manuscript accepted to Combustion Science and Technology, DOI: 10.1080/00102202.2018.1521394
CONTACT S. E. Yakush. Email: yakush@ipmnet.ru

theoretically. Unstable pulsed combustion at high flowrates and spin combustion at certain conditions were obtained experimentally by Zamashchikov (2003, 2006).

Fundamental interest to premixed flame propagation in narrow gaps is stimulated by research into intrinsic flame instability, a topic which has been studied extensively over the past decades. It is known that different instability types affect premixed flames, contributing to formation of cellular structure. The Darrieus-Landau hydrodynamic instability theory predicts that plane flame front is unconditionally unstable at any wavelength, while nonlinear effects cause stabilization of smooth elements (cells) separated by angular points (cusps) on the flame surface (Zeldovich *et al.* 1985; Bychkov and Liberman 2000; Matalon 2007; Clavin and Searby 2016). Diffusional-thermal instability theory (Sivashinsky 1977) predicts cell formation for Lewis number (i.e., ratio of thermal conductivity to diffusivity of the deficient reactant) below a critical value close to unity. Other instability types contributing to the evolution of premixed flame front are the Rayleigh-Taylor instability due to buoyancy of hot combustion products, and the Saffman-Taylor instability attributed to the viscosity jump across the flame front (see the overview in Fernández-Galisteo *et al.* (2018)). Cells are dynamic structures exhibiting irregular motion, merging and reappearance (e.g., (Bradley and Harper 1994; Kuznetsov and Minaev 1996)).

Since many linear and non-linear factors contribute to the development and evolution of cells and cracks on the flame surface, their studies are of high interest in the combustion theory, being a continuing focus of numerous experimental and theoretical works. In this respect, flame propagation in a narrow gap between parallel plates (the Hele-Shaw cell) is an important case where many features of flame instability can be studied more readily than in open space. Such flames are quasi-2D (Joulin and Sivashinsky 1994), which facilitates their experimental observation and theoretical analysis. Note that in the Hele-Shaw setup (narrow gap between two plates of lateral dimensions much larger than the gap width) the flame itself remains three-dimensional due to the no-slip conditions and thermal losses caused by the presence of walls. Large aspect ratio between the lateral and transverse sizes leaves enough degree of freedom for the flame to develop instabilities in comparison with quasi-1D channels and tubes, where the perturbations on the flame front are limited in size by the tube diameter. This makes the problem feature-rich, while remaining advantageous from the measurement, visualization, and interpretation points of view in comparison with open space flames.

A linear theory of a quasi-2D premixed flame propagation in a narrow gap was proposed by Joulin and Sivashinsky (1994), where effects of heat and momentum losses due to presence of walls were analyzed. In (Song *et al.* 2006; Pizza *et al.* 2008), 2D simulations of flame development after ignition by a hot kernel were performed in a channel cross-section normal to the plates, so that no account for flame wrinkling in the transverse direction was made. Fernández-Galisteo *et al.* (2015, 2018) developed a quasi-2D model based on averaging the flow properties across the cell gap in the limit of Peclet number (ratio of gap width to thermal flame thickness) tending to zero. In this model, only momentum losses were taken into account by Poiseuille flow assumption, whereas heat losses were suppressed by the adiabatic wall assumption. Numerical simulations revealed the dynamics of propagating flame front and instability development, variation of problem parameters allowed the relative importance of various instability mechanisms to be evaluated. The results obtained were in good qualitative and (in some cases) quantitative agreement with the experiments by Wongwiwat *et al.* (2015). An alternative approach to the theoretical analysis of flame instability in narrow gap is to solve the Sivashinsky equation, which was shown to provide good agreement with

experimental observations in (Al-Sarraf *et al.* 2017).

In order to validate various theoretical and numerical models, and have an insight into the details of flame instability development for real fuels, direct experimental measurements and observations are required. Despite the evident advantages mentioned above, experimental studies of premixed flame propagation in narrow gaps available so fare are not too numerous. Generally, in the Hele-Shaw experiments, facilities of larger dimensions (of the order of 1 m) were used, and flames were propagating in initially quiescent fuel-air mixtures. Larger facility size is important because it provides sufficient propagation time and distance for flame front instability to develop.

A Hele-Shaw cell with the combustion chamber 59.5 cm long, 39.5 cm wide and 0.5-inch thick was used by Wongwiwat *et al.* (2015) to study flame propagation in H_2-O_2-N_2 mixtures at different Lewis numbers. Mixture was ignited by three sparks, producing diverging flames which rapidly merged into a single front propagating to the other end of the Hele-Shaw cell. By varying the concentrations of hydrogen, oxygen, and nitrogen, a range of equivalence ratios was obtained, with the Lewis number varying from Le = 0.3 for fuel-rich mixture (when hydrogen is the deficient component) to 1.3 for lean mixtures where O_2 is the stoichiometrically limiting reactant. Contribution of different instability mechanisms was identified, and differences in the flame shape caused by variation of Lewis number, mixture strength (adiabatic flame temperature) and propagation direction (upward, downward, horizontal) were revealed.

A similar experimental facility of about twice larger sizes was used by Almarcha *et al.* (2015); Al-Sarraf *et al.* (2017) to study the effect of gap width on the characteristics of a linear flame propagating in a Hele-Shaw cell. The burner consisted of two glass plates 0.50 m wide and 1.5 m high, experiments were conducted with lean (equivalence ratio 0.9) and stoichiometric propane-air mixtures with two gap widths of 4.7 or 3.8 mm. The experimental procedure included arranging a bottom-fed flow of air and propane with the desired equivalence ratio, and establishing an inverted V-flame in the top part of the burner. After that, the flow was stopped, and the downward flame propagation was recorded by a high-speed camera. From the measured data, cell growth rates were determined as functions of the wave number of perturbations. The experimental results also suggest that heat losses effects are more pronounced than Saffman-Taylor friction effects.

In the experimental works by Samsonov *et al.* (2011); Alekseev *et al.* (2011); Alexeev *et al.* (2017), a horizontal Hele-Shaw cell was formed by two 60-cm diameter glass disks; stoichiometric and fuel-rich premixed propane and methane flames were studied at different equivalence ratios. Unlike the experiments by Wongwiwat *et al.* (2015); Almarcha *et al.* (2015); Al-Sarraf *et al.* (2017), ignition was performed by a spark at a single point near the disk center, so that the flame front propagated radially, rather than linearly. The diverging flame shape was registered by high-speed video camera, and the effects of gap on the visible flame propagation speed were evaluated. An interesting experimental finding in Samsonov *et al.* (2011); Alekseev *et al.* (2011) was that for very rich (near-upper limit) propane-air mixtures a single cylindrical flame appearing after ignition rapidly disintegrated into a number of individual rotating flame kernels propagating along curved trajectories (the spin combustion mode).

Thus, previous experimental and theoretical results imply that flame instability in narrow channels is a self-developing process, an intrinsic flame feature of combustion which exhibits itself even in the absence of external flow perturbations or temperature gradients.

This goal of this work is the experimental study of laminar flame instability in a narrow gap between two parallel plates (Hele-Shaw cell), with the emphasis on

establishing the dependence of visible flame speed on the gap width, visualization of flame propagation pattern revealing the temporal evolution of the cellular structure, as well as on the study of the effect of ignition point (central and non-central ignition) on the flame propagation patterns.

2. Experimental Setup

2.1. *Facility*

The facility for studying the laminar flame propagation in narrow gaps is sketched in Fig. 1. The facility is similar to that used by Samsonov *et al.* (2011); Alekseev *et al.* (2011); Alexeev *et al.* (2017), the difference being that provision for non-central ignition was added, and more sophisticated processing of results was performed.

The channel walls were formed by two parallel glass disks (1) of 60 cm diameter, the upper one was solid, the lower one had five round holes (2) of 2 cm diameter located on a single diameter (one central hole and two holes at distances of 10 and 20 cm on both sides from the disk center). The holes were intended for spark ignition at different positions, during the experiments they were plugged flush with the plate surface to avoid gas outflow or inflow, as well as to minimize possible disturbances to the flame.

The gap width between the disks was variable in the range of 2-8 mm, the desired distance was set by three calibrated washers installed on the periphery of the disks, the thickness of each washer was controlled to the accuracy of 0.001 mm. Experiments reported in this paper were conducted with twenty gap widths in the range $H = 2.5 - 4.4$ mm.

Mixture ignition was performed by a high-voltage spark powered by ignition coil (3), the distance between the electrodes (6) was 1.5 mm. The igniter was attached to one of the plugs and could be located in any hole in the bottom plate. Ignition was performed after a delay of about 30 sec after filling the space between the plates with fuel-air mixture, in order to let the mixture become quiescent after the filling process. The system was open, i.e., at the periphery the space between the disks was connected to atmosphere, therefore, combustion occurred at constant (atmospheric) pressure.

Flame propagation was recorded either by a video camera Xiaomi Yi or by a photo camera Canon EOS 30D (5) installed above the center of the disks. Xiaomi Yi camera has Sony IMX206 16 megapixel 6.17×4.55 mm CMOS image sensor which allows recording video at 120 frames per second with 1280×720 resolution. Video camera was installed at a height of 455 mm above the discs. Due to its short 2.66 mm focal length and ultra wide-angle lens, the camera produces pictures with strong visual distortion which was corrected afterwards by the built-in software algorithms. On the corrected video frames, the visible difference between two reference 1 cm-long straight lines placed at the center and periphery of the disk was within one pixel, and each pixel corresponded to 0.87 mm. The photo camera Canon EOS 30D with 18 mm focal length was mounted at a height of 840 mm above the discs. Canon EOS 30D has 22.5×15.0 mm CMOS sensor with effective sensor resolution of 8.2 megapixels. The photo camera was operated in two modes, with a short-time exposure (1/500 s) to provide the instantaneous visible flame shape, or with the open shutter, providing long-exposure pictures equivalent to overlaying of a large number of still photos. The latter allows one to trace the evolution of cellular flame structure over the whole process of flame propagation. All experiments were carried out in a dark room to

avoid background light interference.

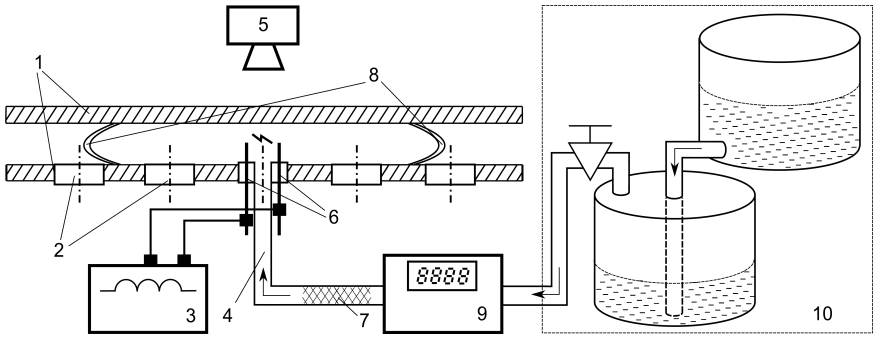

Figure 1. Sketch of experimental facility: top and bottom glass plates (1), plugged round holes in the bottom plate (2), ignition coil (3) , mixture supply hose (4), high-speed video or photo camera (5), spark electrodes (6), flame extinguisher (7), radially diverging flame front (8), gas volume meter (9), two-tank displacement gas meter (10).

2.2. *Mixture Properties and Experimental Parameters*

Experiments were performed with stoichiometric and fuel-rich propane-air mixtures (the equivalence ratio was in the range $\phi = 1.0 - 1.25$). Lean mixtures were difficult to ignite in the narrow channels considered here, their study was beyond the scope of the present work.

Fuel-air mixture of a given concentration was prepared in the displacement gas meter (10 in Fig. 1) to the relative accuracy of 2%, it was supplied into the space between the plates (1) through a hose (4) attached to the central hole and equipped with a porous flame extinguisher (7). The displacement gas meter consisted of two 50-liter tanks connected by a hose, allowing preparation of 42 liters of combustible mixture. The volume of supplied gas (measured by the gas supply meter (9)) was at least 3 liters, the actual volume of supplied fuel-air mixture was increased with the gap width, so that the ratio of supplied gas to the volume of chamber was above 2 to ensure proper filling. Fuel concentration was controlled only during the preparation of mixture.

In order to evaluate the non-dimensional parameters characterizing the mixture (most importantly, the effective Lewis number) and experimental conditions (Peclet number), properties of the C_3H_8-O_2-N_2 mixture were calculated. For individual species, the specific heat capacity $c_{p,i}$, specific enthalpy h_i as functions of temperature were calculated from polynomial approximations using the database from the GRI-MECH 3.0 detailed combustion mechanism. Transport properties, including the conductivity λ_i and binary diffusion coefficient for each pair of species D_{ij}, were evaluated from the molecular kinetics theory (Hirschfelder *et al.* 1964). The mixture specific heat $c_p = \sum Y_i c_{p,i}$, conductivity $\lambda = \frac{1}{2}\left(\sum X_i\lambda_i + 1/\sum X_i/\lambda_i\right)$, density ρ, thermal conductivity $\alpha = \lambda/c_p\rho$, and mixture-averaged diffusion coefficient $D_i^m = (1-Y_i)/\left(\sum_{j\neq i} X_i/D_{ij}\right)$ were obtained (here, X_i and Y_i stand for the mole and mass fraction of i-th species, respectively). Since the oxidizer is a stoichiometrically deficient reactant in fuel-rich flames, the Lewis number was evaluated as $\mathrm{Le} = \alpha/D^m_{\mathrm{O}_2}$).

Calculations were performed for three values of the equivalence ratio $\phi = 1.0$, 1.1, and 1.25 from the experimental range, with the ratio of mole fractions of oxidizer and

neutral species corresponding to air ($X_{O_2}/X_{N_2} = 21/79$). The results obtained for two temperatures, the ambient one, $T_0 = 300$ K, and a characteristic temperature in the preheating zone, $T_m = 1500$ K, are summarized in Table 1. Also, the laminar flame propagation velocity, S_L, is given for each mixture, based on the data by Zhao *et al.* (2004). One can see that the flames studied here are characterized by Lewis number less than unity, albeit rather close to the theoretical stability boundary Le = 1 (Joulin and Sivashinsky 1994). This means that diffusional-thermal instability can affect the flame front. Note that the mixture properties and the resulting Lewis number depend on the composition very weakly, in contrast to hydrogen flames studied by Wongwiwat *et al.* (2015).

Table 1. Properties of propane-air mixture at different ϕ (^{a} at $T_0 = 300$ K, ^{b} at $T_m = 1500$ K).

ϕ	$X_{C_3H_8}$, %	S_L, cm/s	α, cm^2/s		$D^m_{O_2}$, cm^2/s		Le	
1.0	4.03	40.4	0.207^a	2.904^b	0.217^a	3.35^b	0.953^a	0.894^b
1.1	4.42	42.0	0.205^a	2.868^b	0.216^a	3.33^b	0.952^a	0.860^b
1.25	5.00	36.6	0.203^a	2.815^b	0.214^a	3.31^b	0.950^a	0.851^b

The thermal thickness of flame front evaluated by the fresh mixture properties is $\delta_T = \alpha/S_L \approx 5.2 \cdot 10^{-2}$ mm. For the gap width of $H = 2.5$–4.4 mm, the corresponding Peclet number $\mathrm{Pe} = H/\delta_T = HS_L/\alpha \approx 45 - 90$. Similar estimates at a characteristic preheating zone temperature $T_m = 1500$ K give $\delta_T \approx 7.2 \cdot 10^{-1}$ mm, Pe = 3.6–6.5. These latter values are low enough to expect that the transverse flame structure is dominated by heat conduction, with the temperature maximum located halfway between the plates, and monotonic temperature decrease towards the walls due to heat losses. This velocity profile in the transverse direction is also expected to be of Poiseuille type because the Reynolds number estimated by the hot gas parameters is quite low: Re = Pe/Pr = 5.1–9.3 (where Pr = 0.7 is the Prandtl number).

2.3. *Processing of Video Recordings*

From each video recording, all frames with flame front were extracted as images and post-processed using the algorithms of OpenCV (2018) library.

Video frames obtained in low light conditions are subject to a high level of noise, so at first the images were blurred using bilateral filter which is highly effective in noise removal while keeping edges on images sharp. The next step of image processing was to convert images of the flame front from RGB to grayscale color space and then apply the threshold by intensity filter. The result of this step is a binary image in which pixels of the flame front are assigned white color value and pixels of the background are set to black color. These two steps allowed us to remove any ambient background noise and foreign objects in the images leaving only the flame front. Parameters of both filters were selected manually to take into account possible variation of light intensity of the background and the flame front which were dependent on the gap width.

Noise and background removal was followed by detection of the outer and inner contours of the flame front using `findContours()` function of OpenCV library which implements the algorithm by Suzuki and Abe (1985). The output of this function applied to binary image is a set of all contours found in the image with information on the nested contours hierarchy. The outer edges of the flame fronts were determined as the contours with the largest area and the inner edges were obtained as the largest

child contours of the outer contours. The contour itself is a set of point coordinates in the image coordinate system. Knowing the coordinates of the flame contour points allowed us to find the minimum enclosing and maximum inscribed circles, as well as coordinates of the angular points (cusps) on the flame front.

The circles of minimum area enclosing the flame front and ignition center was found on each video frame with `minEnclosingCircle()` OpenCV library function to which the point sets of the outer flame contours were passed.

In order to obtain the coordinates of flame front cusps, for each frame the Cartesian coordinates of contour points were converted to polar coordinates with the origin at the ignition point. As a result, the flame front was represented by a mathematical function $r = r(\phi)$ given by the table, where ϕ is an angle from the reference direction, and r is the distance from the ignition point to the flame front outer edge in this direction. Some smoothing was applied to the ordered sets of distances r in full 360° range of polar angle ϕ to remove picture noise remaining after the first steps of image processing. Cusps were identified as the local minima of $r = r(\phi)$ function. Each local minimum of the function was found by simple comparison of r values of each point to r values of several adjacent points ahead with a specified minimum difference.

The radius of the largest inscribed circle for each flame front was acquired as the global minimum of the function representing the edge of the flame front in polar coordinates.

The coordinates of local minima obtained were converted back to the image Cartesian coordinate system and drawn as points on each separate video frame, together with the contours and circles, to visually verify the correctness of image processing. One such frame is presented in Fig. 2, where locations of the angular points (cusps) derived from image processing are marked by dots, the minimum enclosing and maximum inscribed circles are also shown.

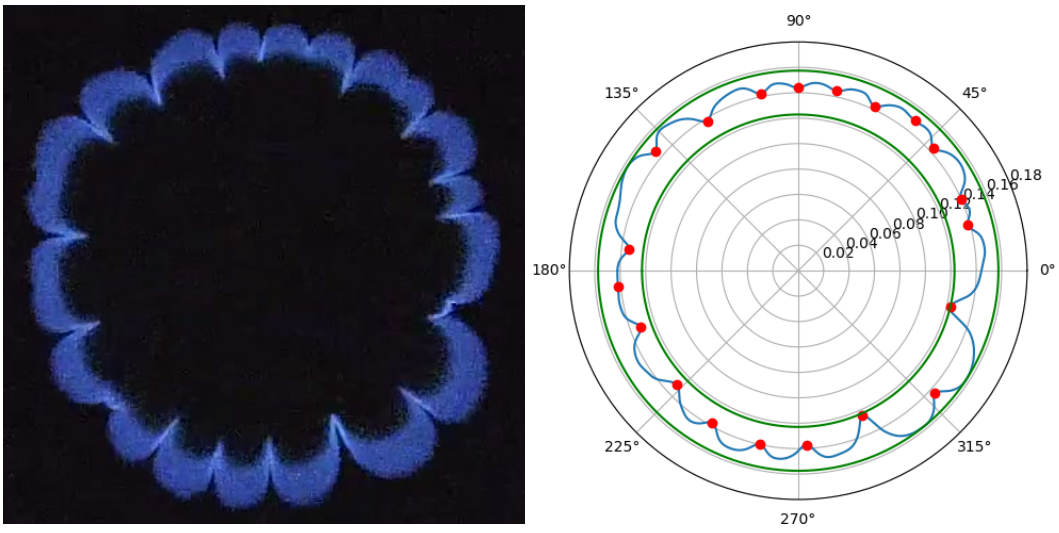

Figure 2. A video frame of the flame front propagating in the gap (left) and processed outer flame front edge represented by a curve in polar coordinates (right).

3. Results

3.1. *Ignition and Initial Flame Evolution*

Spark ignition was performed at one or two locations where plugs equipped with igniters were inserted in the bottom plate (see Fig. 1). Straight after ignition, several flow speed oscillations, visible as rapid flame acceleration and deceleration, were observed. Such behavior was limited to the flame radii of few centimeters, and the flame front at this stage was practically cylindrical, without any well-defined cells. After the flame traveled some 5 cm and cellular structures developed, video recordings revealed steady radial propagation of the cellular flame without noticeable speed oscillations. Note beforehand that in the long-exposure photos revealing the history of cellular flame propagation to be presented in Section 3.4, flame speed oscillations were limited to the dark areas around the ignition points, see Figs. 12 - 14.

An example of the case where flame speed oscillations were recorded is propagation of a 5% propane-air flame ($\phi = 1.25$) in a gap of width $H = 3.4$ mm, see Fig. 3. One can see that initial rapid expansion is followed by flame arrest at time about 0.035 s, with few further flame accelerations and decelerations visible as damped flame speed oscillations; the flame speed stabilizes at about 0.5 m/s by the time 0.15 s. The characteristic period of these flame speed oscillations is about $\Delta t_f \approx 0.05$ s. For the facility radius of $R_0 = 0.3$ m, the characteristic acoustic time based on the speed of sound in air at normal conditions $c_s = 330$ m/s is $\Delta t_s = R_0/c_s = 9.1 \cdot 10^{-4}$ s, i.e., $\Delta t_f/\Delta t_s \approx 50$. This clearly indicates that the oscillations observed are not of acoustic nature, but are caused by low-Mach flame development and changes in its thermal, concentration, and velocity structure.

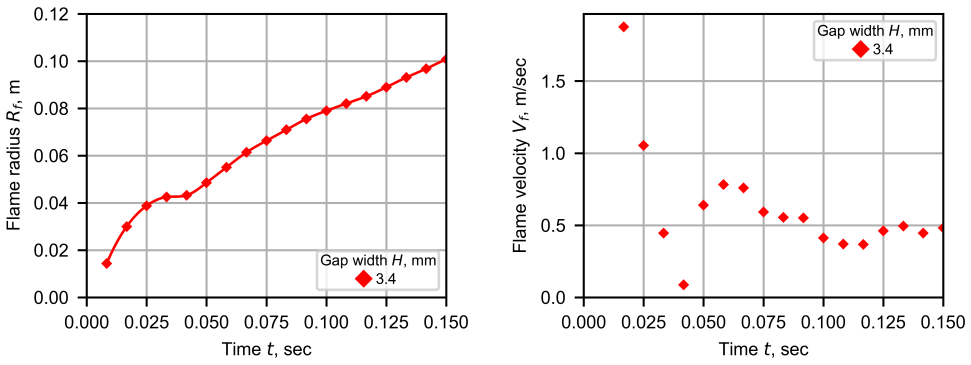

Figure 3. Time histories of flame radius (left) and instantaneous flame speed (right) during the first few centimeters of flame propagation (5% propane-air mixture).

One of the possible reasons for this behavior was discussed by Bychkov *et al.* (2007); Akkerman *et al.* (2010) when considering the flame propagation after ignition in round tubes. It was obtained that, due to the presence of solid walls with no-slip conditions, the flow velocity profile is non-uniform across the tube cross-section, causing stretching of the flame front and increase in the flame surface area, increasing the effective burning rate and causing flame acceleration. It should be noted that numerical results revealing this behavior were obtained by Bychkov *et al.* (2007); Akkerman *et al.* (2010) under the assumption of adiabatic walls, i.e., without heat losses. Interaction of the combustion zone with cold walls could contribute to the flow oscillations at

the intitial stage, during which self-consistent flowfield, temperature and concentration distributions were establishing. The heat losses slowing down combustion in the gas immediately adjacent to the cold wall are diminishing the effects of flame surface enhancement due to Poiseuille-type velocity profile, thus limiting the number and strength of oscillations. Detailed study on the flame oscillations straight after ignition, and comparison with existing theories was beyond the scope of this work where we focused on the cellular flames traveled far enough from the ignition point.

3.2. *Cellular Flame Propagation*

Consider first the results obtained for 4.0% propane-air flames ($\phi = 1.0$) propagating in gaps of different width H = 2.4–4.8 mm. Note that the lower limit of the range corresponds to the narrowest gap at which a steadily propagating flame could be obtained, flames in smaller gaps were extinguished shortly after ignition.

A typical shape of the flame propagating outwards from the ignition point is shown in Fig. 4 for three values of gap width H = 2.5 (a), 3.0 (b), and 4.4 (c) mm; on each plate the flame fronts taken from video frames with time step of 80 ms (a, b) and 10 ms (c) are overlayed. It can be seen that the flame assumes cellular structure shortly after ignition. For the two smaller gap widths, the wrinkled flame contains a number of large-scale cells, each containing several smaller cells. Also clearly visible are the angular points separating the cells. A distinct feature of the flame propagating in the wider gap (c) is that the cells are more regular and stable, and smaller-scale wrinkling the large-scale cells was not observed.

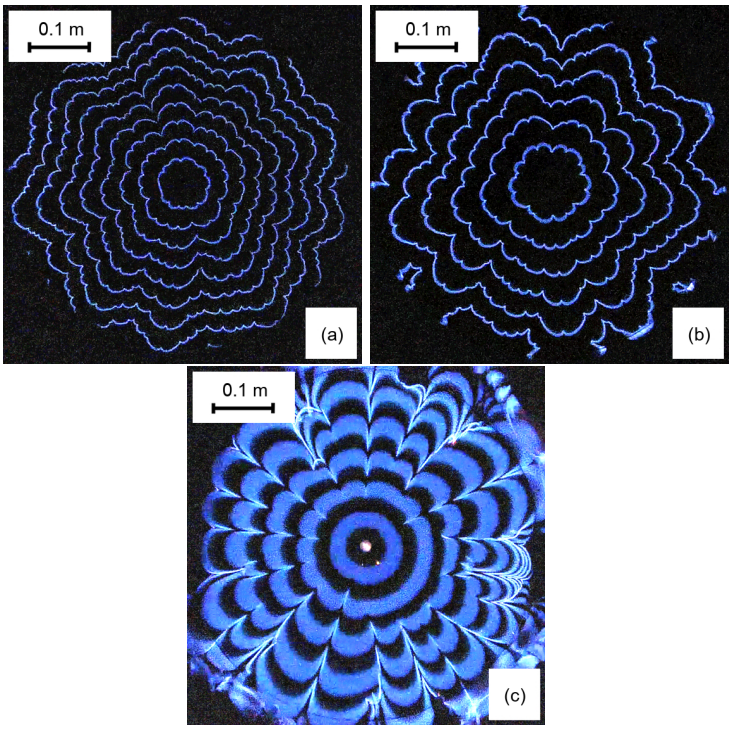

Figure 4. 4% propane-air flames propagating in gaps of different width: H = 2.5 mm (a), 3.0 mm (b), 4.4 mm (c).

Experiments show that, the narrower the gap, the slower the visible flame propa-

gation. Two factors contribute to the variation of visible flame speed.

Firstly, the classical theory of flame propagation in a tube with cold walls (Zeldovich *et al.* 1985) predicts the reduction in the flame speed due to the heat losses from the flame to the cold walls and to the combustion products behind the flame. Heat losses reduce the temperature in the combustion zone and, accordingly, the normal flame speed; the effect becoming more pronounced with the decrease in the tube diameter. For flames propagating between closely spaced parallel plates, the effect of gap width is qualitatively the same: the narrower the gap, the higher the relative effect of heat losses on the flame temperature and normal flame speed. Note that direct measurement of heat losses was not possible with the instrumentation available in the experimental facility.

Secondly, upon the central ignition studied here, the visible flame speed is affected by the expansion of combustion products behind the flame. Unlike the ideal case of an adiabatic flame, where the visible flame speed is higher than the normal flame speed by a factor depending on the gas expansion ratio (or the temperature ratio of burnt and fresh gas), in the presence of cold channel walls the combustion products are cooling behind the flame and, therefore, the gas is shrinking, also reducing the visible flame speed, see discussion in (Joulin and Sivashinsky 1994).

In order to obtain the dynamics of flame propagation in a narrow gap, 20 video recordings obtained for the same mixture (4% propane in air) in various gaps were processed.

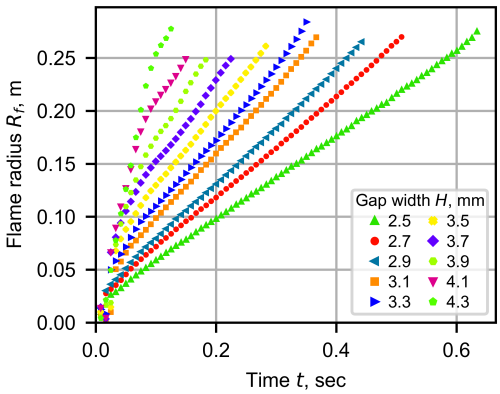

Figure 5. Time histories of the outer flame radius R_f for different gap width (4% propane-air mixture).

In Fig. 5, the time histories of outer flame radius R_f (i.e., the radius of minimum enclosing circle) are shown for different gap widths. Evidently, in each case the flame propagates at a constant velocity V_f which can be derived as the slope of the corresponding line $R_f(t)$. The results are presented in Fig. 6 which indicates that flame propagation becomes faster as the gap width exceeds 4 mm. The error bars indicated on the points for higher propagation velocities correspond to the RMS error of linear regression.

By taking the laminar flame propagation speed for stoichiometric propane-air mixture $S_L = 0.4$ (see Table 1), we can conclude from Fig 6 that at the smallest gap width of 2.5 mm, the visible flame speed practically coincides with S_L. For the widest gap, the acceleration factor reaches $V_f/S_L = 8.8$. Note that a wider range of velocity ratios was obtained experimentally in (Wongwiwat *et al.* 2015; Fernández-Galisteo *et al.*

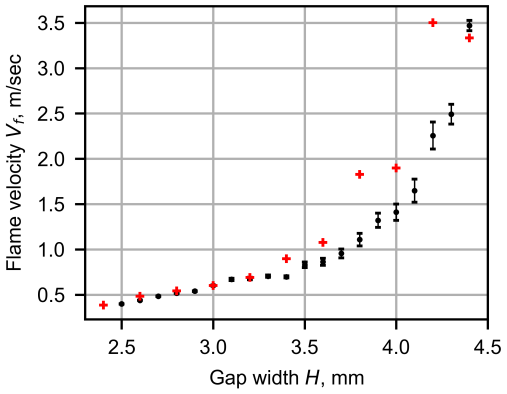

Figure 6. Flame velocity V_f as a function of gap width H (4% propane-air mixture). Crosses correspond to an additional test series performed for repeatability study.

2018) for hydrogen flames, but in those experiments the initial mixture composition was varied significantly, which affected not only the visible flame speed, but also S_L.

Since cellular flames exhibit random behavior due to instability development and flame fronts never repeat themselves even if the tests are performed at exactly the same mixture concentration and gap width, an important question is how representative the results on flame propagation speed presented in Fig. 6 are. In order to evaluated the repeatability of results, an additional series of experiments was performed. In this series, some tests were repeated with the same concentration and gap width, but results were processed manually, by finding the inscribed and circumscribed circles for the flame front at ten selected instants; the flame speed was then found by linear regression. The results obtained are shown in Fig. 6 by crosses. One can see that for the gap width of $H = 2.4$–3.3 mm repeatability is very good (within 1%), with further increase in the gap width up to 3.6 mm the difference increases to some 10%, while for wider gaps (above 3.8 mm) repeatability deteriorates (interestingly, for the widest 4.4 mm gap result agree fairly well again). It will be shown in the next section that for the gap width above 4.2 mm some other peculiarities in fame characteristics are also observed, which might indicate that random effects become quite strong, explaining the just-mentioned repeatability deterioration.

3.3. *Cell Size*

Comparison of the flame snapshots presented in Fig. 4 shows that the cells developing in narrower gaps are of smaller spatial scales than those developing in wider gaps. Since the process of cell formation due to flame instability is random, of interest are statistical characteristics of the cells; such data can be used for validation of instability theories and numerical simulations.

In order to obtain the quantitative characteristics of cells developing on the flame front propagating in narrow gaps, each snapshot processed in Figs. 5 and 6 was also used to determine the total number of cells on the flame front, N_c, mean lateral cell size $L_c = 2\pi R_f/N_c$, as well as the radial size of flame front perturbation $\Delta_f = R_f - r_f$ (where r_f is the radius of the incircle) and its relative value Δ_f/R_f.

Results of this analysis are presented in Figs. 7–8 for the lateral cell size, and in

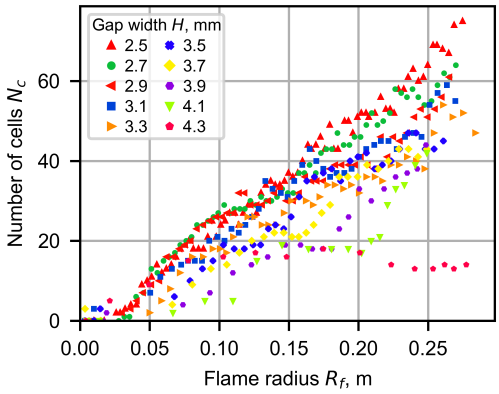

Figure 7. Number of cells N_c on the flame front as a function of flame outer radius R_f.

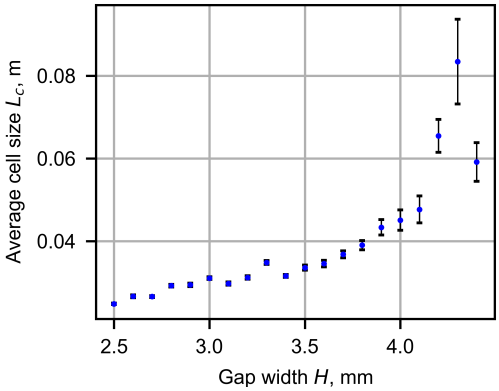

Figure 8. Average cell size L_c as a function of gap width H.

Figs. 10–11 for the radial disturbances of flame front. Importantly, the lateral and radial amplitude of flame perturbations (of the of the order of 2–5 centimeters in all cases) is much larger than the gap width (few millimeters), see Fig. 9 where the ratio of cell size to gap width, L_c/H, is plotted. Though the cells look quasi-two-dimensional, the flame remains three-dimensional due to the transversal velocity and temperature gradients in the narrow channel.

Note that for the gap sizes of 4.2 and 4.3 mm, the radial and circumferential cell sizes obtained are rather big, deviating significantly from the main trend. Exact reasons for this are not clear, nevertheless these results were not discarded from the graphs. For the wider gaps flames propagated at much higher speeds (see Fig. 6), which requires higher frame rates than those provided by the camera used in this work for reliable flame shape registration. Such experiments, together with repetability tests, might shed light on this peculiarity in flame propagation.

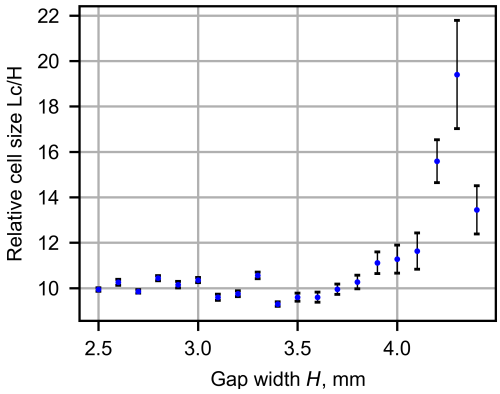

Figure 9. Relative cell size L_c/H as a function of gap width H.

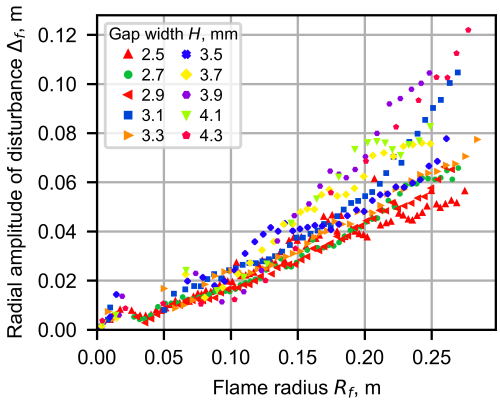

Figure 10. Radial amplitude of flame front perturbations Δ_f as a function of flame radius R_f.

3.4. *Long-exposure Flame Patterns*

The whole process of flame propagation can be better understood by overlaying a large number of instantaneous frames revealing the trajectories of characteristic points of the flame. This was achieved by repeating the experiments with the video camera Xiaomi Yi substituted by the photo camera Canon EOS 30D. The photo camera was operated with long exposure time, i. e., the shutter was kept open for a long enough period, and the resulting photos contained the recording of glowing area over the given time (equivalent to overlaying multiple instantaneous snapshots).

In Fig. 12, the long-exposure picture is shown for 5% propane-air flame (equivalence ratio $\phi = 1.25$), the gap width was $H = 2.8$ mm, the exposure time was 0.5 s. The outer boundary of the glowing area corresponds to the instantaneous flame shape at the final moment, the linear scale can be judged by the five circles visible along the diagonal, they correspond to the plugged holes in the bottom plate with the separation distance of 10 cm. Analysis of Fig. 12 enables one to establish the following characteristic features of flame propagation.

(1) Clearly visible are lines, some spanning all the way from inception point to the

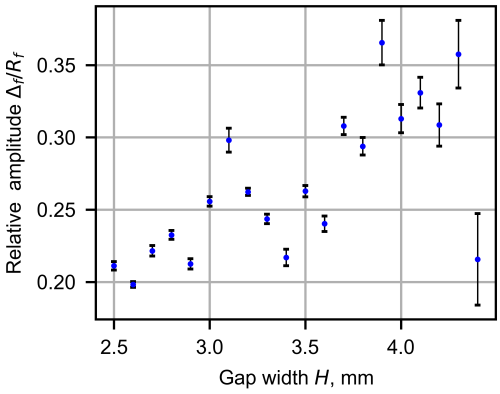

Figure 11. Relative radial amplitude of perturbations Δ_f/R_f as a function of gap width H.

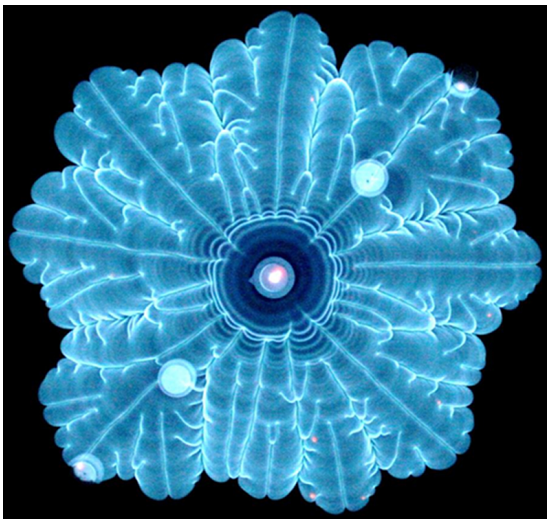

Figure 12. Long-exposure photo of 5% propane flame propagating in a 2.8 mm gap, exposure time 0.5 s.

current front position, some merging and forming triple or higher-order points where cells were appearing and disappearing due to flame instability. Note that, unlike the familiar snapshots of cellular flames in free space, the troughs are not the actual "cracks" on the flame surface; rather, they are the trajectories of angular points (cusps).

(2) Significant flame instability develops only at a distance of about 5 cm from the ignition point, which justifies that experiments on flame instability must be carried out in large enough experimental facility. Flame behavior close to the ignition point was discussed in Section 3.1.

(3) The structures (cells) developing upon the flame propagation are of multiple scales, with the largest cells being more stable than the smaller-scale ones. The lateral size of the large cells is of the order of 2.5 cm, which by far exceeds the transversal scale limited by the gap width of 2.8 mm.

Longer-exposure photos enable us to see the whole process of flame propagation in the experimental facility, until complete fuel burnout. Of interest is to compare

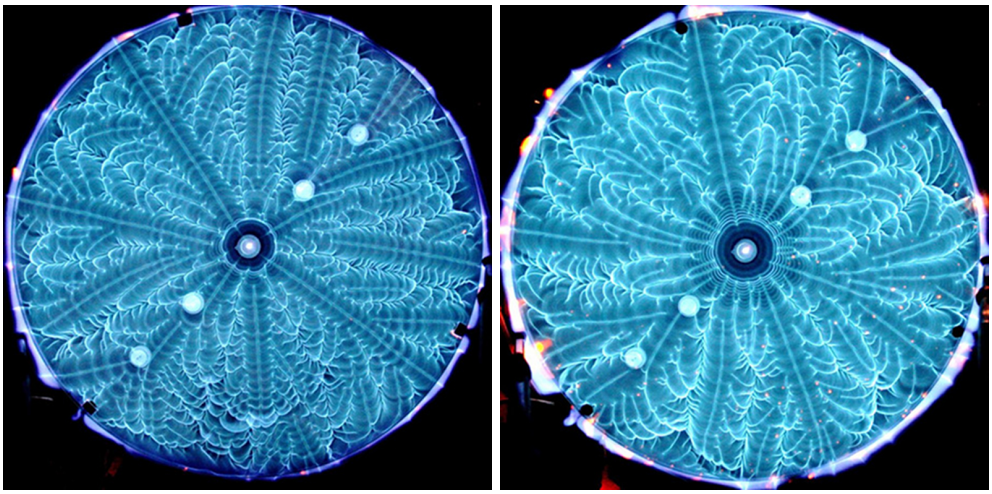

Figure 13. Long-exposure photo of 5% propane flame propagating in a 2.6 mm (left) and 2.9 mm (right) gap, exposure time 1.0 s.

the patters developing upon combustion of the same fuel mixture in gaps of different width. In Fig. 13, the photos obtained for the gap widths of $H = 2.6$ and 2.9 mm are presented. A common feature of both patterns is the presence of long-living perturbations (troughs) creating a rather regular pattern, and of irregular short-living perturbations filling the space between them. Also, it can be seen that when the flame passes the plugged holes, perturbations are generated due to surface roughness, often resulting in either beginning of a new long line, or splitting of a line into two new lines.

3.5. *Non-central Ignition*

In order to study the effect of ignition point location on the flame propagation between parallel plates, few experiments were carried out where combustion was initiated by a spark at one of the side holes in the bottom disk. Here, we present the results obtained for ignition at one or two holes farthest from the disk center, the corresponding flame propagation patterns are shown in Fig. 14 for 5% propane-air mixture ($\phi = 1.25$), the gap width was $H = 2.9$ mm.

For ignition at the leftmost hole (left picture in Fig. 14), the exposure time was 0.6 s, so that the instantaneous flame front can be seen as the boundary of the glowing area. An interesting finding is that the flame did not propagate in a radial manner. Instead, a "bird-like" pattern developed, with well-defined "wings" at the periphery of the disks. A possible explanation to faster flame propagation in this area is that some mixing occurred near the outer edge of the disks contacting with the ambient air, bringing the fuel concentration closer to stoichiometric and, thus, increasing the flame speed in comparison with that in the central area of the plates where no such additional mixing occurred.

Simultaneous ignition at two outmost points (right picture in Fig. 14) results in quite a symmetric flame propagation pattern, with the transversal line where both flames met clealy visible, passing right through the center of the plate. Otherwise, the general features of the cellular flame structure (presence of long-living lines, scale of the cells) is very similar between these two cases, as well as very similar to that obtained for central ignition, see Fig. 13 (right plate).

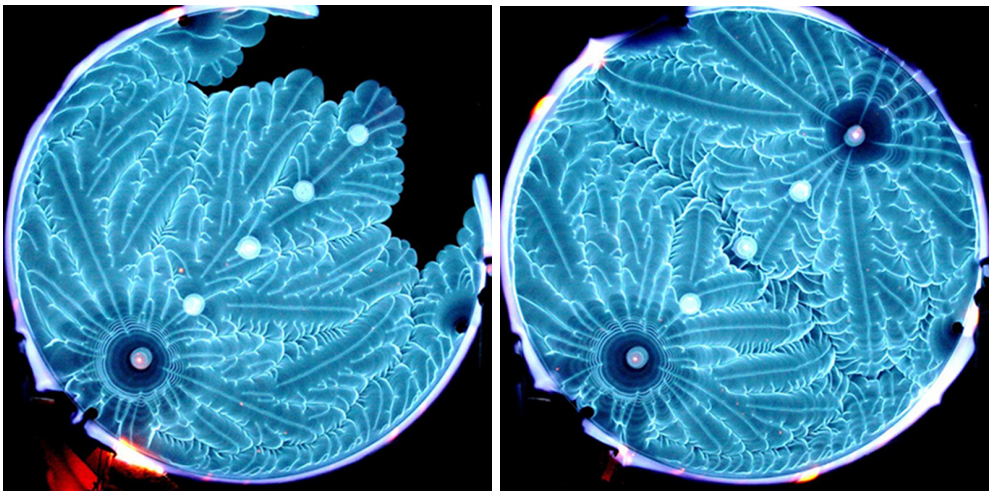

Figure 14. Long-exposure photos of flame propagation in 5% propane-air mixture, gap width $H = 2.9$ mm, non-central ignition at one point (left, exposure time 0.6 s) and two symmetric points (right, exposure time 1.2 s).

4. Discussion on Instability Mechanisms

Four instabilty types which can affect premixed quasi-2D flame propagation in Hele-Shaw configuration were discussed by Wongwiwat *et al.* (2015); Fernández-Galisteo *et al.* (2015, 2018). Their relative role was clarified by changing the Lewis number in H_2-O_2-N_2 mixtures by varying the equivalence ratio and mixture strength (characterized by the adiabatic flame temperature), as well as comparing the results obtained for upward, horizontal, and downward flame propagation. This approach was successful because of large differences in the reactant diffusivities, which allowed a wide range of Lewis numbers (from 0.3 to 1.3) to be covered.

In the current experiments, the focus was on the effect of gap width between the plates on the visible flame propagation velocity, as well as on the visualization of global flame propagation patterns. The equivalence ratio was varied in rather narrow range, $\phi = 1.0$–1.25, and the Lewis number was nearly constant, slightly below unity (see Table 1). It can be argued that the two main instability types affecting the development of cellular flame are the Darrieus-Landau (DL) hydrodynamic instability, and the diffusional-thermal (DT) instability. Indeed, the flame front shapes obtained are generally featured by cusped cells, with spontaneously developing disturbances leading to competing appearance and merging of cells. Interestingly, the flame propagation patterns, especially in the space between the main troughs, closely resemble those obtained experimentally and numerically in (Wongwiwat *et al.* 2015; Fernández-Galisteo *et al.* 2015, 2018) at low Lewis numbers (Le = 0.3).

It is difficult to judge on the basis of results obtained on the separate effect and relative importance of Saffman-Taylor (ST) instability. However, a numerical study on the effect of heat and momentum loss performed by Kang *et al.* (2006) suggests that DT instability mechanism is primarily responsible for splitting into smaller flame cells, while the DL and ST mechanisms favor larger flame cells through merging. Also, it was found in (Kang *et al.* 2006) that heat losses increase the growth rate of perturbations, which is consistent with finer-scale cells obtained in the current work in narrower gaps (see Fig. 13).

Experiments presented in this work were carried out in a gap between horizontal plates, therefore, Raleigh-Taylor (RT) did not play any significant role.

5. Conclusions

Experiments on flame propagation in narrow gaps (Hele-Shaw cell) provide unique possibilities for insight into flame instability and cellular structure. Despite this, experimental data on the effect of gap width on the development of cellular flame instability and on the flame propagation velocity in a planar channel formed by two parallel plates are very scarce, in contrast to a much better studied case of flame propagation in a round tube. For example, in (Wongwiwat *et al.* 2015) experiments were performed in a fixed-width channel (0.5 inch), while in (Al-Sarraf *et al.* 2017) only two gap widths, 3.8 and 4.7 mm, were used. The main novelty of the results presented in the current paper is that a systematic experimental study on the premixed flame propagation in 20 channels of 2.5–4.4 mm width was performed, revealing i) the effect of gap width on the visible flame velocity, and ii) flame propagation patterns demonstrating the global evolution of cells upon the whole flame propagation process, presented as continuous trajectories of characteristic flame points unavailable when a limited number of still photo images are superimposed (e.g., in (Wongwiwat *et al.* 2015) only four images were combined, revealing the flame shapes at the corresponding instants, rather than a continuous flame propagation pattern).

The experimental results presented in this work show that flame propagation in a narrow gap between parallel walls is a complex process where flame instability manifests itself in the development of flame cells. Visualization of flame propagation patterns achieved by taking long-exposure photos clearly confirms that the cellular structure is subjected to irregular motion, formation and merging of cells.

Because of intrinsic randomness involved in cell evolution, of particular interest are statistical features of the flames, including the average visible flame speed, and size distribution of the cells developing throughout the whole process of flame propagation. These quantities, in particular, provide a quantitative way for validation of theoretical models and numerical simulations. So far, numerical simulations of flames propagating in narrow gaps were limited to 2D or quasi-2D setup (e.g., (Song *et al.* 2006; Pizza *et al.* 2008; Fernández-Galisteo *et al.* 2018)). Direct numerical simulations of 3D flame structure can provide an insight into flame instability mechanisms and features, including the quantitative estimation of heat losses to cold channel walls (some first attempts to model methane flames with detailed chemical mechanism were performed in (Alexeev *et al.* 2017)). Further experimental work will be focused on the studies of different fuels, gravity effects, and widening the range of equivalence ratios to obtain the boundaries where flame disintegration into separate kernels (spins) occurs in different configurations.

Acknowledgments

This research was supported by Russian Foundation for Basic Research, Grant No. 16-01-00557.

References

Akkerman, V., Law, C.K., Bychkov, V., and Eriksson, L.E., 2010. Analysis of flame acceleration induced by wall friction in open tubes, *Physics of Fluids*, 22 (5), 1–14.

Al-Sarraf, E., Almarcha, C., Radisson, B., Denet, B., and Quinard, J., 2017. Flame instability in a Hele-Shaw cell: thickness effect, *in: Proceedings of the 8th European Combustion Meeting ECM2017*, Dubrovnik, Croatia, 18-21 April, 2017, 357–360.

Alekseev, M.M., Smirnova, I.V., and Samsonov, V.P., 2011. Spinning front formation in fuel gas-air flame, *Technical Physics Letters*, 37 (4), 330–332.

Alexeev, M., Borisov, V., Semenov, O., and Yakush, S., 2017. Instability of laminar flame propagation in a narrow gap between parallel plates, *in: Proceedings of the 8th European Combustion Meeting ECM2017*, Dubrovnik, Croatia, 18-21 April, 2017, 2034–2039.

Almarcha, C., Quinard, J., Denet, B., Al-Sarraf, E., Laugier, J.M., and Villermaux, E., 2015. Experimental two dimensional cellular flames, *Physics of Fluids*, 27 (9), 9–11.

Bradley, D. and Harper, C.M., 1994. The development of instabilities in laminar explosion flames, *Combustion and Flame*, 99 (3-4), 562–572.

Bychkov, V., Akkerman, V., Fru, G., Petchenko, A., and Eriksson, L.E., 2007. Flame acceleration in the early stages of burning in tubes, *Combustion and Flame*, 150 (4), 263–276.

Bychkov, V.V. and Liberman, M.A., 2000. Dynamics and stability of premixed flames, *Physics reports*, 325 (4-5), 115–237.

Clavin, P. and Searby, G., 2016. *Combustion Waves and Fronts in Flows: Flames, Shocks, Detonations, Ablation Fronts and Explosion of Stars*, Cambridge University Press.

Fan, A., Minaev, S., Kumar, S., Liu, W., and Maruta, K., 2008. Regime diagrams and characteristics of flame patterns in radial microchannels with temperature gradients, *Combustion and Flame*, 153 (3), 479–489.

Fan, A., Minaev, S., Sereshchenko, E., Fursenko, R., Kumar, S., Liu, W., and Maruta, K., 2009. Experimental and numerical investigations of flame pattern formations in a radial microchannel, *Proceedings of the Combustion Institute*, 32 II (2), 3059–3066.

Fernández-Galisteo, D., Gross, J., Kurdyumov, V.N., and Ronney, P.D., 2015. Premixed flame propagation between two closely spaced parallel plates, *in: 25th ICDERS*, Leeds, UK, 1–6.

Fernández-Galisteo, D., Kurdyumov, V.N., and Ronney, P.D., 2018. Analysis of premixed flame propagation between two closely-spaced parallel plates, *Combustion and Flame*, 190, 133–145.

Hirschfelder, J.O., Curtiss, C.F., and Bird, R.B., 1964. *Molecular Theory of Gases and Liquids*, Wiley.

Joulin, G. and Sivashinsky, G.I., 1994. Influence of momentum and heat losses on the large-scale stability of quasi-2D premixed flames, *Combustion Science and Technology*, 98 (1-3), 11–23.

Ju, Y. and Maruta, K., 2011. Microscale combustion: Technology development and fundamental research, *Progress in Energy and Combustion Science*, 37 (6), 669–715.

Kang, S.H., Baek, S.W., and Im, H.G., 2006. Effects of heat and momentum losses on the stability of premixed flames in a narrow channel, *Combustion Theory and Modelling*, 10 (4), 659–681.

Kuznetsov, E.A. and Minaev, S.S., 1996. Formation and propagation of cracks on the flame surface, *Physics Letters A*, 221, 187–192.

Matalon, M., 2007. Intrinsic flame instabilities in premixed and nonpremixed combustion, *Annual Review of Fluid Mechanics*, 39 (1), 163–191.

Minaev, S., Fursenko, R., and Maruta, K., 2007. Stability of cylindrical flame in radial micro channel with a wall temperature gradient, *in: 21st ICDERS*, Poitiers, France, July 23-27, 1–4.

Minaev, S., Fursenko, R., Sereshchenko, E., Fan, A., and Kumar, S., 2013. Oscillating and rotating flame patterns in radial microchannels, *Proceedings of the Combustion Institute*, 34 (2), 3427–3434.

OpenCV, 2018. *Open Source Computer Vision Library, v. 3.4*, `https://opencv.org`.

Pizza, G., Frouzakis, C.E., Mantzaras, J., Tomboulides, A.G., and Boulouchos, K., 2008. Dynamics of premixed hydrogen/air flames in mesoscale channels, *Combustion and Flame*, 155 (1-2), 2–20.

Samsonov, V.P., Alexeev, M.M., and Smirnova, I.V., 2011. Mechanism of spin flame front formation, *Phys. Usp.*, 54 (9), 931–937.

Sivashinsky, G.I., 1977. Diffusional-thermal theory of cellular flames, *Combustion Science and Technology*, 37 (3-4), 137–146.

Song, Z.B., Ding, X.W., Yu, J.L., and Chen, Y.Z., 2006. Propagation and quenching of premixed flames in narrow channels, *Combustion, Explosion and Shock Waves*, 42 (3), 268–276.

Suzuki, S. and Abe, K., 1985. Topological structural analysis of digitized binary images by border following, *Computer Vision, Graphics, and Image Processing*, 30 (1), 32–46.

Wongwiwat, J., Gross, J., and Ronney, P.D., 2015. Flame propagation in narrow channels at varying lewis number, *in: 25th ICDERS*, Leeds, UK, 3–8.

Zamashchikov, V.V., 2003. Rotating gas flames, *Combustion, Explosion and Shock Waves*, 39 (2), 124–125.

Zamashchikov, V.V., 2006. Spin gas combustion in a narrow slot, *Combustion, Explosion and Shock Waves*, 42 (3), 264–267.

Zeldovich, Ya.B., Barenblatt, G.I., Librovich, V.B., and Makhviladze, G.M., 1985. *The Mathematical Theory of Combustion and Explosions*, New York: Consultants Bureau.

Zhao, Z., Kazakov, A., Li, J., and Dryer, F.L., 2004. The initial temperature and N2 dilution effect on the laminar flame speed of propane/air, *Combustion Science and Technology*, 176 (10), 1705–1723.